Physics of thermo-acoustic sound generation

M. Daschewski,[a] R. Boehm, J. Prager, M. Kreutzbruck, and A. Harrer
Federal Institute for Materials Research and Testing (BAM), Unter den Eichen 87, 12205 Berlin, Germany

(Received 6 August 2013; accepted 27 August 2013; published online 18 September 2013)

We present a generalized analytical model of thermo-acoustic sound generation based on the analysis of thermally induced energy density fluctuations and their propagation into the adjacent matter. The model provides exact analytical prediction of the sound pressure generated in fluids and solids; consequently, it can be applied to arbitrary thermal power sources such as thermophones, plasma firings, laser beams, and chemical reactions. Unlike existing approaches, our description also includes acoustic near-field effects and sound-field attenuation. Analytical results are compared with measurements of sound pressures generated by thermo-acoustic transducers in air for frequencies up to 1 MHz. The tested transducers consist of titanium and indium tin oxide coatings on quartz glass and polycarbonate substrates. The model reveals that thermo-acoustic efficiency increases linearly with the supplied thermal power and quadratically with thermal excitation frequency. Comparison of the efficiency of our thermo-acoustic transducers with those of piezoelectric-based airborne ultrasound transducers using impulse excitation showed comparable sound pressure values. The present results show that thermo-acoustic transducers can be applied as broadband, non-resonant, high-performance ultrasound sources. © *2013 AIP Publishing LLC*. [http://dx.doi.org/10.1063/1.4821121]

I. INTRODUCTION

Thermo-acoustic sound generation occurs in many forms such as thunder, underwater spark discharge (used in medical extracorporeal shock wave lithotripsy), plasma loudspeakers, laser-induced sound excitation, and thermophones (which use thin ohmic conductors to generate sound upon the application of an electric current).

The advantages of thermophones over conventional ultrasound transducers are their broadband and resonance-free behavior, simple construction, and low production costs.

Experimental attempts to use the thermo-acoustic effect for sound generation by thermophones date back to the beginning of the 20th century. In 1915, De Lange used 7-μm-thin platinum wires as a telephone receiver,[1] and Arnold and Crandall[2] in 1917 used a 700 nm-thin platinum film as a precision sound source for calibrating microphones. Wente[3] proposed in 1922 the use of a thermophone for measuring the thermal conductivity of gases. In 1933, Geffcken and Keibs[4] used thermophones to study the acoustic threshold of human hearing. In 1999, Shinoda *et al.*[5] first proposed the use of a 30 nm-thin aluminum film on porous silicon as an airborne ultrasonic source, and Boullosa and Santillan[6] showed in 2004 that such a conductive film on a wood, kapton, or mica substrate is also suitable for ultrasound generation. In 2008, Xiao *et al.* used a carbon nanotube (CNT) film as a stretchable loudspeaker,[7] and tested it two years later as a low-frequency (<100 kHz) ultrasound source in argon and helium gases.[8] In 2009, Niskanen *et al.*[9] used a suspended aluminum wire array and reached a sound pressure level of 110 dB at 40 kHz in air at a distance of 8 cm in front of the transducer. Another use of CNTs is the work of Aliev *et al.* showing that CNTs might be used for underwater sound generation.[10] In 2011, Tian *et al.*[11] tested different graphene sheets on paper substrates. They also recently presented 100 nm ITO coatings on PET (polyethylene terephthalate) and glass substrates,[12] and investigated their performances for frequencies up to 50 kHz.

All previous theoretical models describing the operation of the above thermo-acoustic devices are based on time-dependent systems of coupled partial differential equations (PDEs) for temperature and pressure. Unfortunately, an exact, purely analytical solution of these PDE-systems is difficult, as many assumptions and simplifications are needed. Therefore, the existing analytical solutions yield similar qualitative results for the generated sound pressures with respect to the input power and excitation frequency, but their use of some different constants and parameters leads to different quantitative results.

For example, Arnold and Crandall[2] predicted a linear dependence of the generated sound pressure on the input power and a square root dependence on the excitation frequency.

Shinoda *et al.*[5] used the model of McDonald and Wetsel[13] for the photo-acoustic effect and proposed, without derivation, a formula that predicts the generated sound pressure to be linearly dependent on the supplied thermal power density.

Boullosa and Santillan[6] compared the heat flux outward from the transducer film to the movement of an imaginary piston, and formulated an equation similar to Shinoda's for the generated sound pressure but with a different dependence on the isentropic expansion factor.

Xiao *et al.*[7,8] modified the formula of Arnold and Crandall, keeping the square root dependence on excitation frequency and proposing the heat capacity per unit area

[a]Email: maxim.daschewski@bam.de

theory (HCPUA) based on their theoretical and experimental results. They concluded that an efficient thermo-acoustic transducer should have a small heat capacity per unit area.

Vesterinen *et al.*[14] formulated an analytical equation very similar to those of Arnold and Crandall[2] and Xiao;[7,8] but obtained a linear dependence of the sound pressure on the input power and excitation frequency. They also used the Finite Difference Method to analyze the frequency and input power dependency of their thermophone by numerically solving the coupled PDEs for temperature and pressure. They concluded that the efficiency of a thermophone depends linear on the supplied thermal power and on the square of the thermal excitation frequency.

The work of Hu *et al.*[15,16] using the same PDE system used by Shinoda *et al.*[5] and Boullosa and Santillan[6] reported similar results. They investigated theoretically the thermal expansion of the conductive film and showed that it is very small and can be neglected.

We can briefly summarize the following points.

(i) The commonly used analytical models for describing the operation of a thermo-acoustic device such as a thermophone predict for the generated sound pressures a linear dependence on the input power and the excitation frequency. However, all models have different constants and parameters and, therefore, yield different results.

(ii) Arnold and Crandall,[2] Xiao *et al.*,[7,8] and Vesterinen *et al.*[14] used the temperature oscillations of the transducer film in their PDEs, and concluded that the transducer film has to be very thin and should have a small heat capacity per unit area.

(iii) The models of Shinoda *et al.*,[5] Boullosa and Santillan,[6] and Hu *et al.*[15,16] use the temperature oscillations of the surrounding gas and arrive at solutions for the generated sound pressure that are, contrary to (ii), independent of the transducer film thickness.

(iv) Only Boullosa and Santillan[6,17] and Xiao *et al.*[8] took into account the size and shape of the transducer.

(v) Published experimental examinations of thermo-acoustic devices such as thermophones have reported frequencies not exceeding 100 kHz, which are far below those commonly used in ultrasonic non-destructive testing applications.

(vi) The previous works have neglected the influence of frequency-dependent sound attenuation due to scattering effects and viscous friction.

In this paper, we present a generalized analytical model of thermo-acoustic sound generation based on the analysis of thermally induced energy density fluctuations (EDFs) and their propagation into the adjacent matter. Using this EDF-based model, we avoid the problems encountered by the analytical solution of nonlinear PDE systems and arrive at an exact, full analytical solution for the generated sound pressure at each point of the adjacent matter, regardless of whether solid or fluid.

The developed EDF-based model enables the analytical prediction of the sound pressure generated in fluids and solids by arbitrary thermal power sources; e.g., chemical reactions, laser beams, plasma firings, and also thermophones. It allows the quantitative three-dimensional prediction of the sound field distribution around a thermo-acoustic sound source of arbitrary size, shape, and material. The model could also be used in the design of targeted transducers for specific applications.

In Sec. IV, the analytical results of our EDF-based model are compared with measurements of the sound pressure generated by electro-thermo-acoustic transducers consisting of titanium and ITO coatings on quartz glass and polycarbonate substrates in air at frequencies of 4 kHz–1 MHz. Laser vibrometry was used to measure sound particle velocity in this broad frequency range.

Our analytical and experimental investigations show that the efficiency of thermo-acoustic sound sources increases linearly with the imparted thermal power and quadratically with the thermal excitation frequency. Consequently, optimized thermo-acoustic transducers can exceed in their efficiency the conventional ultrasound transducers, and could greatly benefit, for example, ultrasound microscopy and other high-frequency ultrasound applications.

II. THEORY

From the thermodynamic point of view, an acoustic wave can be considered to have the following properties.

1. It is a closed thermodynamic system of finite volume V that transports energy at sound velocity without any mass transportation.
2. The mean value of the pressure p inside the sound wave corresponds to the mean value of its internal energy density,

$$p \equiv \check{U}/V. \tag{1}$$

3. Given the first law of thermodynamics, the change of internal energy $\Delta\check{U}$ of a closed thermodynamic system is equal to the sum of the heat ΔQ supplied to the system and the volume-work ΔW performed on it,

$$\Delta\check{U} \equiv \Delta Q + \Delta W = \Delta Q - p \times \Delta V. \tag{2}$$

Conventional acoustic transducers, such as loudspeakers and piezoelectric transducers, move bidirectionally and compress or expand the adjacent medium adiabatically. They do not generate heat ($\Delta Q = 0$), and only perform adiabatic volume-work $\Delta W = -p \times \Delta V$. In this way, they generate a periodic variation of internal energy $\Delta\check{U} = \Delta W$, and hence a variation of pressure amplitudes Δp. However, a solid vibrating transducer like a piezoelectric transducer or a membrane is a mass–spring system, and this leads to drawbacks such as a frequency-dependent amplitude response and large post-oscillations in the case of impulse excitation.

Thermo-acoustic transducers work without any macroscopic moving parts and displacement of their surface; therefore, they do not perform any mechanical volume-work, $\Delta W = 0$. They generate heat ΔQ, which is equal to the change of internal energy $\Delta\check{U}$. This local variation of the

internal energy leads to a variation of pressure $\Delta p = \Delta \check{U}/V$, which in turn generates a sound wave. (The mechanism of sound wave genesis using a thermal power source is covered more fully in Appendix A.)

In the following, we first consider a thermophone consisting of an electrically conductive film, a solid substrate, and an adjacent fluid. For this three-layer setup, we derive a formula for the amplitude of the generated sound pressure depending on the time function of the supplied electric power. Subsequently, we derive a formula for free-hanging conductive wires or foils, which is also applicable to plasma sound sources. These formulae can also be used for the determination of sound pressure generated by an arbitrary thermal power source with known surface and thermal power time function.

Let us consider a homogeneous, few nanometers thin, electrically conductive film of area S_{film} and a purely ohmic resistance R on a smooth and homogeneous solid substrate in a semi-infinite fluidic space.

Assuming the film is excited by a sinusoidal voltage without offset $U_{el}(t) = U \times \sin(\omega \times t)$, with $\omega = 2 \times \pi \times f$ and frequency f, the electric current is, therefore, also a sine function $I_{el}(t) = I \times \sin(\omega \times t) = U \times \sin(\omega \times t)/R$.

Note that for the low-megahertz range we neglect the electrical skin effect, which gives a penetration depth for electrical current; e.g., in titanium, on the order of a few 100 μm. Thus, we can suppose a homogeneous current distribution along the cross-section of the film.

The converted electric power $P_{el}(t)$, which is equal to the thermal power, is the product of these two functions and has double the frequency of the originally supplied voltage and current,

$$\begin{aligned} P_{el}(t) &= U \times \sin(\omega \times t) \times I \times \sin(\omega \times t) \\ &= U \times I \times \sin^2(\omega \times t) \quad = R \times I^2 \times \sin^2(\omega \times t) \\ &= R \times I^2 \times \left(1 - \cos(2 \times \omega \times t)\right)/2\,. \end{aligned} \tag{3}$$

In this case, the effective value of electric power corresponds to

$$P_{el\,eff} \quad = U \times I/2\,. \tag{4}$$

When the film is excited by a sinusoidal voltage with offset $U_{el}(t) = U \times (1 + \sin(\omega \times t))$, the electric current is $I_{el}(t) = I \times (1 + \sin(\omega \times t)) = U \times (1 + \sin(\omega \times t))/R$, and the corresponding electric power

$$\begin{aligned} P_{el}(t) &= U \times (1 + \sin(\omega \times t)) \times I \times (1 + \sin(\omega \times t)) \\ &= R \times I^2 \times (1 + \sin(\omega \times t))^2 \\ &= R \times I^2 \times (1 + 2 \times \sin(\omega \times t) - (1 - \cos(2 \times \omega \times t))/2) \\ &= R \times I^2 \times (1 + 4 \times \sin(\omega \times t) + \cos(2 \times \omega \times t))/2 \end{aligned} \tag{5}$$

contains the excitation frequency and its first harmonic.

Figure 1 shows examples of the corresponding electric power and generated sound pressures for both kinds of excitation.

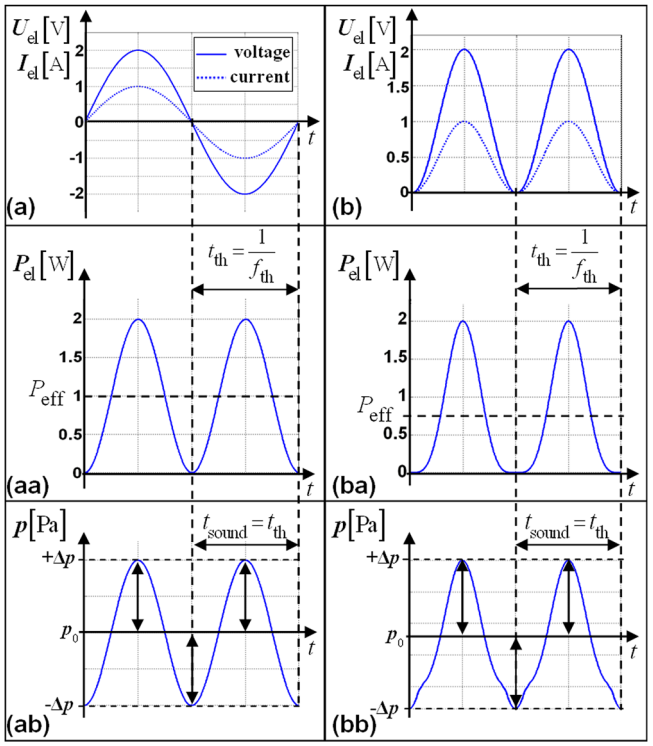

FIG. 1. Time profiles of electric power (aa, ba) and (ab, bb) the corresponding generated sound pressures for (a) sinusoidal excitation without offset $U_{el}(t) = U \times \sin(\omega \times t)$, and (b) sinusoidal excitation with offset $U_{el}(t) = U \times (1 + \sin(\omega \times t))$.

The time functions of the generated sound waves $\Delta p(t)$ in the substrate, as well as in the fluid, correspond to the function of the outward heat flux and hence to the function of the supplied electric power,

$$p(t) \sim \dot{Q}(t) = P_{el}(t). \tag{6}$$

The doubling of frequency when a sine voltage without offset is applied is a characteristic property of electro-thermo-acoustic transducers.

Hence, for the generation of a single-frequency tone free from any harmonics distortion, the transducer should be driven by a sinusoidal voltage without offset at half the desired frequency.

When alternating electric power converted inside the transducer film has a constant offset larger than the alternating amplitude, e.g., $P_{el}(t) = P_{ac} \times (1 + \sin(\omega \times t)) + P_{dc}$, only the alternating part P_{ac} is converted into sound waves. The P_{dc} part of the electric power constantly heats the transducer film, substrate, and the surrounding fluid; produces acoustical noise; and is removed by photonic radiation, conduction, and convection.

Another important point is that the pressure amplitude of the generated sound wave depends on the instantaneous thermodynamic state of the transducer film and the adjacent matter. That is, when the transducer film, the surrounding fluid, and the substrate are, for example, at a certain constant temperature $T_0 \sim \check{U}_0$ an excitation with a short power impulse generates a positive pressure impulse.

When the transducer is excited with a continuous sinusoidal electric power with constant effective value P_{eff}, the

transducer film, the substrate, and also the surrounding fluid close to the transducer will all be heated. After reaching the thermodynamic equilibrium temperature T_{eq} (for determination of T_{eq} see Appendix B), the transducer generates positive and negative pressure changes like a conventional transducer (see Figs. 1(ab) and 1(bb)). The reason for this behavior is that the internal energy of the transducer film, adjacent substrate, and fluid now alternates around the equilibrium value of $\check{U}_{eq} = Q_{eff} \sim P_{eff}$, and so $\Delta\check{U}(t) = Q_{eff} \times \sin(\omega \times t)$ has "negative" and "positive" parts.

For a quantitative determination of the generated sound pressure $\Delta p(t_{th}) = \Delta Q(t_{th})/V(t_{th})$ during a heating period t_{th}, we need to determine:

(i) the amount of heat $Q_{th\,in}$ generated in the transducer film during one heating period t_{th} and its distribution between the transducer film, substrate, and adjacent fluid; and
(ii) the volume of generated sound wave in the considered radiation direction.

A. Distribution of generated thermal energy $Q_{th\ in}$ during a heating period t_{th}

In general,

$$Q_{th\,in} = \int_0^{t_{th}} P_{el}(t)dt \tag{7}$$

but using the effective value of the supplied electric power $P_{el\ eff}$, we obtain a simplified equation for the amount of heat generated during one heating period t_{th},

$$Q_{th\,in} = P_{el\,eff} \times t_{th} = P_{el\,eff}/f_{th}. \tag{8}$$

The heating of the transducer film leads to photonic radiation and heat flux into the adjacent fluid and substrate, leading to the energy balance

$$Q_{th\,in} = Q_{film\,th} + Q_{sub\,th} + Q_{fluid\,th} + Q_{photons\,th}. \tag{9}$$

For a film surface S_{film} smaller than a few square centimeters and a temperature increase of the film up to 100 °C, less than 0.1% of the input energy $Q_{th\,in}$ is converted into photonic radiation $Q_{photons\,th}$ during one heating period t_{th}. (For determination of $Q_{photons\,th}$ see Appendix C.) Thus, we can neglect the $Q_{photons\,th}$ and the energy balance is simplified to

$$Q_{th\,in} = Q_{film\,th} + Q_{sub\,th} + Q_{fluid\,th}. \tag{10}$$

The amounts of thermal energy distributed between the transducer film ($Q_{film\,th}$), substrate ($Q_{sub\,th}$), and fluid ($Q_{fluid\,th}$) are proportional to their thermal capacities (see also Fig. 2). This analogy to the electrical capacity of electrical charges is well established.

The thermal capacity of a transducer film C_{film} is equal to the product of its thickness d_{film}, surface area S_{film}, specific heat capacity $c_{p\ film}$, and density ρ_{film}

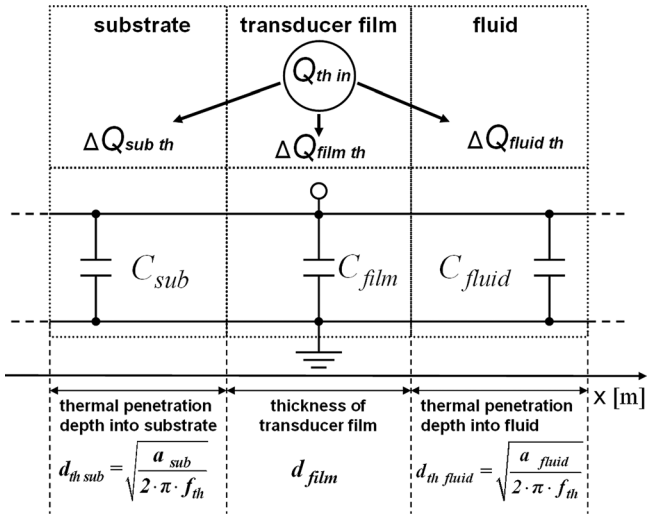

FIG. 2. Distribution of the thermal energy $Q_{th\,in}$ generated inside a transducer film.

$$C_{film} = d_{film} \times S_{film} \times \rho_{film} \times c_{p\,film}. \tag{11}$$

The heat capacities of the adjacent fluid and substrate depend on their frequency-dependent thermal penetration depths $d_{th}(f_{th})$,

$$\begin{aligned} C_{fluid}(f_{th}) &= d_{th\,fluid}(f_{th}) \times S_{film} \times \rho_{fluid} \times c_{p\,fluid} \\ &= \sqrt{\frac{a_{fluid}}{2 \times \pi \times f_{th}}} \times S_{film} \times \rho_{fluid} \times c_{p\,fluid} \\ &= \sqrt{\frac{\lambda_{fluid}}{\rho_{fluid} \times c_{p\,fluid} \times 2 \times \pi \times f_{th}}} \times S_{film} \times \rho_{fluid} \times c_{p\,fluid} \\ &= \sqrt{\frac{\lambda_{fluid} \times \rho_{fluid} \times c_{p\,fluid}}{2 \times \pi \times f_{th}}} \times S_{film} = \frac{e_{fluid} \times S_{film}}{\sqrt{2 \times \pi \times f_{th}}}, \end{aligned} \tag{12}$$

$$\begin{aligned} C_{sub}(f_{th}) &= d_{th\,sub}(f_{th}) \times S_{film} \times \rho_{sub} \times c_{p\,sub} \\ &= \sqrt{\frac{a_{sub}}{2 \times \pi \times f_{th}}} \times S_{film} \times \rho_{sub} \times c_{p\,sub} \\ &= \sqrt{\frac{\lambda_{sub}}{\rho_{sub} \times c_{p\,sub} \times 2 \times \pi \times f_{th}}} \times S_{film} \times \rho_{sub} \times c_{p\,sub} \\ &= \sqrt{\frac{\lambda_{sub} \times \rho_{sub} \times c_{p\,sub}}{2 \times \pi \times f_{th}}} \times S_{film} = \frac{e_{sub} \times S_{film}}{\sqrt{2 \times \pi \times f_{th}}}, \end{aligned} \tag{13}$$

with thermal diffusion $a = \lambda/(\rho \times c_p)$ and thermal effusivity $e = \sqrt{\lambda \times \rho \times c_p}$, where λ is the heat conductivity, ρ the density, and c_p the specific heat capacity of the material.

The amount of thermal energy flowing from the transducer film into the substrate and the fluid $Q_{out} = Q_{fluid} + Q_{sub}$ is related to the total generated energy $Q_{th\,in}$ (see Eq. (10)) by

$$\frac{Q_{fluid} + Q_{sub}}{Q_{th\,in}} = \frac{C_{fluid} + C_{sub}}{C_{fluid} + C_{sub} + C_{film}}, \tag{14}$$

and

$$Q_{out} = Q_{fluid} + Q_{sub} = Q_{th\,in} \times \frac{C_{fluid} + C_{sub}}{C_{fluid} + C_{sub} + C_{film}}. \quad (15)$$

The relationship of the thermal energy flowing into the fluid (Q_{fluid}) to the amount of thermal energy flowing into the substrate (Q_{sub}) is given by

$$\frac{Q_{fluid}}{Q_{sub}} = \frac{C_{fluid}}{C_{sub}} = \frac{e_{fluid}}{e_{sub}}. \quad (16)$$

From Eqs. (15) and (16), and $Q_{sub} = Q_{out} - Q_{fluid}$ it follows that the amount of thermal energy Q_{fluid} flowing into the fluid during one heating period $t_{th} = 1/f_{th}$ is given by

$$\begin{aligned} Q_{fluid\,th} &= Q_{out\,th} \times \frac{C_{fluid}}{C_{fluid} + C_{sub}} \\ &= Q_{th\,in} \times \frac{C_{fluid}}{C_{fluid} + C_{sub}} \times \frac{C_{fluid} + C_{sub}}{C_{fluid} + C_{sub} + C_{film}} \\ &= Q_{th\,in} \times \frac{C_{fluid}}{C_{fluid} + C_{sub} + C_{film}} \\ &= Q_{th\,in} \times \frac{e_{fluid}}{e_{fluid} + e_{sub} + d_{film} \times \rho_{film} \times c_{p\,film} \times \sqrt{2 \times \pi \times f_{th}}}, \end{aligned} \quad (17)$$

and that the amount of thermal energy Q_{sub} flowing into the substrate is given by

$$\begin{aligned} Q_{sub\,th} &= Q_{out\,th} \times \frac{C_{sub}}{C_{fluid} + C_{sub}} \\ &= Q_{th\,in} \times \frac{C_{sub}}{C_{fluid} + C_{sub}} \times \frac{C_{fluid} + C_{sub}}{C_{fluid} + C_{sub} + C_{film}} \\ &= Q_{th\,in} \times \frac{C_{sub}}{C_{fluid} + C_{sub} + C_{film}} \\ &= Q_{th\,in} \times \frac{e_{sub}}{e_{fluid} + e_{sub} + d_{film} \times \rho_{film} \times c_{p\,film} \times \sqrt{2 \times \pi \times f_{th}}}. \end{aligned} \quad (18)$$

For simplification, we now define the energy distribution coefficients E for the fluid and substrate as

$$E_{fluid} = \frac{e_{fluid}}{e_{fluid} + e_{sub} + d_{film} \times \rho_{film} \times c_{p\,film} \times \sqrt{2 \times \pi \times f_{th}}} \quad (19)$$

and

$$E_{sub} = \frac{e_{sub}}{e_{fluid} + e_{sub} + d_{film} \times \rho_{film} \times c_{p\,film} \times \sqrt{2 \times \pi \times f_{th}}}. \quad (20)$$

B. Determination of the volume of a sound wave generated by a point source

Because sound waves propagate at the speed of sound, the volume of the generated sound wave depends on the sound velocity c of the medium and the heating time t_{th}. In the following, we assume an acoustical point source; i.e., the film dimension is at least five times smaller than the length of the generated sound wave. Furthermore we assume a large, plain, and homogeneous substrate and a homogeneous and isotropic surrounding fluid. Figure 3 depicts the propagation of the sound wave away from the source as a spherical longitudinal wave; during the heating time t_{th} it fills a half sphere of volume V_{fluid} with a radius $c_{fluid} \times t_{th}$,

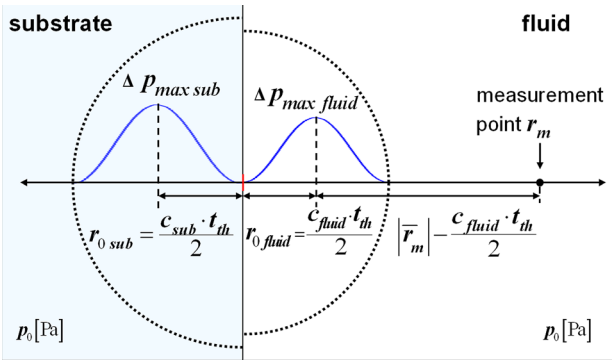

FIG. 3. Schematic representation of the formation of longitudinal sound waves in the fluid and substrate after a sinusoidal excitation with period t_{th} by a thermo-acoustic point source transducer.

$$V_{fluid\,th} = \frac{4}{3} \times \pi \times (c_{fluid} \times t_{th})^3/2 = \frac{2}{3} \times \pi \times (c_{fluid}/f_{th})^3. \quad (21)$$

To determine the volume of the generated sound wave in the substrate, only the parameter for sound velocity c_{sub} has to be substituted in Eq. (21),

$$V_{sub\,th} = \frac{4}{3} \times \pi \times (c_{sub} \times t_{th})^3/2 = \frac{2}{3} \times \pi \times (c_{sub}/f_{th})^3. \quad (22)$$

C. Determination of the sound pressure amplitude generated by a point source

The amplitude of the generated sound pressure in the fluid follows from Eq. (1), and using Eq. (21) we have

$$\Delta p_{fluid}(t_{th}) = \frac{3 \times Q_{fluid\,th}}{2 \times \pi \times (c_{fluid} \times t_{th})^3}. \quad (23)$$

Using the thermal excitation frequency $f_{th} = 1/t_{th}$, Eq. (17) for $Q_{fluid\,th}$, and Eq. (8) for $Q_{th\,in}$, we obtain the following expression for the amplitude of the generated sound wave in the fluid:

$$\Delta p_{fluid}(f_{th}) = \frac{3 \times P_{el\,eff}/f_{th}}{2 \times \pi \times (c_{fluid}/f_{th})^3} \times E_{fluid}. \quad (24)$$

The amplitude of the sound pressure generated by a point source decreases with distance according to the inverse distance law,

$$\Delta p(r) = \Delta p(r_0) \times \frac{r_0}{r}, \quad (25)$$

where

$$r_0 = \frac{c \times t_{th}}{2} = \frac{c}{2 \times f_{th}}, \tag{26}$$

and due to the sound attenuation law,

$$\Delta p(r) = \Delta p(r_0) \times \exp(-\alpha \times (r - r_0)). \tag{27}$$

For sound attenuation in fluids, the Stokes–Kirchhoff attenuation coefficient is used

$$\alpha = \frac{(2 \times \pi \times f_{th})^2}{2 \times \rho_{fluid} \times c_{fluid}^3} \times \left(\frac{4}{3}\mu_d + \mu_v + \lambda \times \left(\frac{1}{c_p} - \frac{1}{c_v}\right)\right), \tag{28}$$

where μ_d is the dynamic and μ_v the volumetric viscosity of the fluid, λ is the heat conductivity, and c_p and c_v are its isobaric and isochoric heat capacities, respectively.

Note that sound attenuation can be neglected for low frequencies in most fluids. For example, the attenuation of a 100 kHz sound wave in air at a distance of 10 cm is on the order of only a few percent, whereas the attenuation at frequencies in the MHz range is a major effect and must be taken into consideration.

Now we can give the complete equation for the amplitude of sound pressure generated by a point source on a substrate driven by sinusoidal excitation without offset for an arbitrary observation point r in the fluid,

$$\Delta p_{fluid}(\bar{r}, f_{th}) = \frac{3 \times P_{el\,eff} \times f_{th}}{4 \times \pi \times c_{fluid}^2 \times |\bar{r}|} \times E_{fluid} \times A_{fluid}, \tag{29}$$

where the sound attenuation factor A_{fluid} is given by

$$A_{fluid} = \exp\left(-\alpha \times \left(|\bar{r}| - \frac{c_{fluid}}{2 \times f_{th}}\right)\right). \tag{30}$$

To determine the sound pressure amplitude generated in the substrate, only the parameters for energy distribution, sound velocity, and sound attenuation have to be changed

$$\Delta p_{sub}(\bar{r}, f_{th}) = \frac{3 \times P_{el\,eff} \times f_{th}}{4 \times \pi \times c_{sub}^2 \times |\bar{r}|} \times E_{sub} \times A_{sub}, \tag{31}$$

where

$$A_{sub} = \exp\left(-\beta \times \left(|\bar{r}| - \frac{c_{sub}}{2 \times f_{th}}\right)\right). \tag{32}$$

To determine the sound pressure generated by free-hanging conductive wires or foils, and also by plasma sound sources, for example, in some homogeneous fluid, the full sphere volume V of the generated sound wave and double the value of e_{fliud} in the energy distribution coefficient E_{fliud} (see Eq. (19)) must be taken into account

$$\Delta p_{fluid}(\bar{r}, f_{th}) = \frac{3 \times P_{el\,eff} \times f_{th}}{8 \times \pi \times c_{fluid}^2 \times |\bar{r}|} \times \frac{e_{fluid}}{(2 \times e_{fluid} + d_{film} \times \rho_{film} \times c_{p\,film} \times \sqrt{2 \times \pi \times f_{th}})} \times A_{fluid}. \tag{33}$$

D. Determination of sound pressure amplitude generated by an extended transducer

For an extended transducer, such as a line, rectangle, or any curved shape, the transducer surface has to be discretized into n point sources (which must be at least five times smaller than the generated sound wavelength). The total thermal input power has to be distributed on all these point sources corresponding to their surface. Using point source synthesis, a discretized version of the Kirchhoff–Helmholtz Integral, the complex amplitudes of all n point sources will be superposed at the observation point r (see Fig. 4(a)).

The absolute value of this superposition yields the sound pressure amplitude Δp at the observation point. So, for example, we get for sound pressure at some point r in a fluid

$$\Delta p_{fluid}(\bar{r}, f_{th}) = \sum_{k=1}^{k=n} \Delta p_{fluid\,k}(\bar{r}_k, f_{th}) \times \left|\exp\left(\mathrm{i} \times 2 \times \pi \times \frac{|\bar{r}_k| \times f_{th}}{c_{fluid}}\right)\right|. \tag{34}$$

Equation (34) is used for the analytical prediction of sound pressure amplitudes at a selected observation point by variation of thermal excitation frequency f_{th} in Figure 6 and for tomographic imaging of generated sound fields by variation of r at a constant excitation frequency in Figure 7.

E. Efficiency of a thermophone on a substrate

In the following, we investigate thermo-acoustic efficiency by generating a sound field with a thermo-acoustic

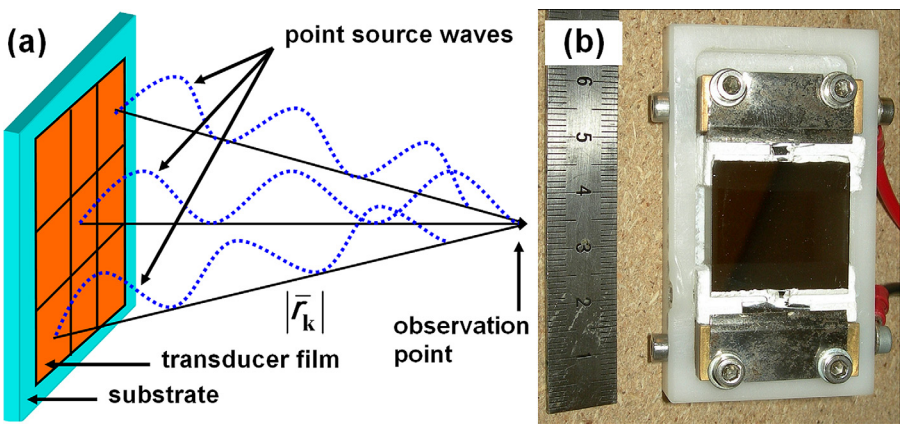

FIG. 4. (a) Schematic representation of point source syntheses. (b) A 20 nm-thin, 22 × 24 mm titanium coating on quartz glass substrate as a transducer sample in a transducer holder.

point source transducer on a substrate driven at a constant effective thermal power.

Following the equation for sound power,

$$P_s(r) = \int_S I_s(r)\, dS = \int_S \frac{\Delta p(r)^2}{Z} dS \tag{35}$$

in which I_s describes the sound intensity and Z the acoustical impedance, we obtain at a certain point r within the far field in a fluid or solid half sphere,

$$P_s(r, f_{th}) = \frac{\Delta p^2(r, f_{th})}{\rho \times c} \times 2 \times \pi \times r^2. \tag{36}$$

Using Eq. (28) for Δp_{fliud}, we obtain the following expression for the power conversion efficiency for sound generation in the fluid,

$$\begin{aligned}\eta_{fluid} &= \frac{P_{s\,fluid}(r, f_{th})}{P_{el\,eff}} \times 100\% \\ &= \frac{9 \times P_{el\,eff} \times f_{th}^2}{8 \times \pi \times \rho_{fluid} \times c_{fluid}^5} \times E_{fluid}^2 \times A_{fluid}^2 \times 100\%. \end{aligned} \tag{37}$$

Using Eq. (31) for Δp_{sub}, we get for the sound generation in the substrate

$$\begin{aligned}\eta_{sub} &= \frac{P_{s\,sub}(\mathrm{r}, f_{th})}{P_{el\,eff}} \times 100\% \\ &= \frac{9 \times P_{el\,eff} \times f_{th}^2}{8 \times \pi \times \rho_{sub} \times c_{sub}^5} \times E_{sub}^2 \times A_{sub}^2 \times 100\%. \end{aligned} \tag{38}$$

Obviously, the efficiency for both fluid and substrate depends *inter alia* linearly on the supplied thermal power $P_{el\,eff}$ and quadratically on the thermal excitation frequency f_{th} when

$$(e_{fluid} + e_{sub})^2 \gg (d_{film} \times \rho_{film} \times c_{pfilm})^2 \times 2 \times \pi \times f_{th}. \tag{39}$$

This condition is well satisfied for film thicknesses up to a few nanometers when using solid substrates and excitation frequencies in the sub-MHz range.

For higher frequencies or thicker transducer film where

$$(e_{fluid} + e_{sub})^2 \approx (d_{film} \times \rho_{film} \times c_{pfilm})^2 \times 2 \times \pi \times f_{th}, \tag{40}$$

the efficiency will depend linearly on both the thermal input power and the thermal excitation frequency.

The thermal power dependence means that the higher the amplitude of the supplied input power, the higher the temperature increase of the transducer film. In turn, this results in an increase of outward heat flux $\dot{Q}(t) = P_{el}(t)$ and an increase of the amount of thermal energy flowing into the fluid and substrate.

The dependence of the efficiency on the thermal excitation frequency means, that the higher the frequency of the fluctuating thermal input power, the smaller the volume of the generated pressure wave.

More thermal energy and a smaller volume both result in increased pressure amplitude, which in turn results in an increase of the sound power.

The maximum achievable efficiency with the thermo-acoustic effect obeys Carnot's law of thermo-mechanical energy conversion,

$$\eta_{thermo-mech\,max} \leq 1 - \frac{T_0}{T_0 + \Delta T_{th\,max}}, \tag{41}$$

where $\Delta T_{th\,max}$ is the maximum temperature difference between the temperature of the generated sound wave and the temperature of its ambient medium T_0.

The temperature $\Delta T_{th\,max}$ of the generated sound wave of volume V in an arbitrary medium of density ρ_m and heat capacity $c_{p\,m}$ can be estimated as follows:

$$\Delta T_{th\,max} = \frac{Q_{m\,th}}{c_{p\,m} \times \rho_m \times V_{wave}} = \frac{P_m \times t_{th}}{c_{p\,m} \times \rho_m \times V_{wave}}. \tag{42}$$

F. Influence of the transducer film materials on the acoustic efficiency

For a better understanding of the influence of the transducer film materials on the efficiency of sound generation, let us neglect the heat conductivity into the adjacent matter and consider an equation for the maximal possible temperature increase of a film of mass m_{film} during a heating period t_{th},

$$\begin{aligned}\Delta T_{th\,film\,max} &= \frac{Q_{th\,in} - Q_{photons}}{c_{p\,film} \times m_{film}} = \frac{(P_{el\,eff} - P_{photons}) \times t_{th}}{c_{p\,film} \times m_{film}} \\ &= \frac{(P_{el\,eff} - P_{photons}) \times t_{th}}{c_{p\,film} \times \rho_{film} \times S_{film} \times d_{film}}. \end{aligned} \tag{43}$$

A given thermo-acoustic transducer of area S_{film} driven by an effective electric power $P_{el\,eff}$ reaches its maximum $\Delta T_{th\,film\,max}$ when the transducer material has the smallest possible heat capacity $c_{p\,film}$, density ρ_{film}, and thickness d_{film}; a small photonic emissivity ε is also required to minimize the amount of energy that will be converted into photonic radiation $Q_{photons}$ (see Appendix C).

This confirms the statement of Arnold and Crandall[2] that the conductor has to be very thin and its heat capacity has to be small. It also confirms the HCPUA theory of Xiao *et al.*[7] that an efficient thermo-acoustic transducer demands a small heat capacity per unit area.

Consequently, it is no surprise that high-frequency plasma combustion, which employs no solid conductor films at all, should have the highest thermo-acoustic efficiency. This explains, for example, why underwater spark discharge—used in extracorporeal shock wave lithotripsy—and thunder are so powerful.

III. EXPERIMENT

For experimental evaluation of the analytical model, we examined the acoustic properties of various transducer samples. Different transducer film materials and different surface areas (4.5×5 mm, 5.5×8 mm, 10×14 mm, 15×20 mm, and 22×24 mm) were compared. Substrates of 1 mm quartz

glass and 5 mm polycarbonate (PC) were coated with electric active layers of 20–300 nm and 30–60 nm, respectively. The substrates were chosen for their well-known properties—density ρ, heat conductivity λ, and specific heat capacity c_p—and also their closed and smooth surfaces, which ensured homogeneous electric conducting layers after coating.

Titanium and ITO conductive films were chosen due to their large electric resistance relative to gold or aluminum, their chemical and thermal stabilities, and their relatively small densities and heat capacities.

Table I summarizes the properties of the substrates, the transducer materials, and the adjacent fluid (air). These values were also used for the analytical prediction of the generated sound pressures.

The heat conductivities and the specific heat capacities of all the materials are temperature dependent and mostly increase with increasing temperature.

The part of the thermal energy flowing into the substrate Q_{sub} also generates sound waves. However, the large reflection coefficient for an acoustic wave at the substrate–air boundary causes these sound waves to travel back and forth within the substrate; the energy contained in acoustic waves is dissipated and constantly heats the substrate and its immediate proximity.

The temperature of the substrate can be determined analytically (see Appendix B) or using a thermometer. For the heat conductivity of the quartz glass substrate, the following approximation was used:[18]

$$\lambda_{glass}(T) = 1.2 + (T - 273.15) \times 7.6 \times 10^{-3}. \quad (44)$$

For air at normal atmospheric pressure, the following linear approximation for heat conductivity was used:[19]

$$\lambda_{air}(T) = 0.0242 + (T - 273.15) \times 7.13 \times 10^{-5}. \quad (45)$$

The electrical resistance R of the conducting film is also temperature dependent. Hence, to determine the supplied electric power $P_{el}(t)$, the amplitudes of the voltage drop $U(t)$ on the film and also of the electric current $I(t)$ were measured simultaneously using an oscilloscope. The electric current $I(t)$ was measured using a 0.1 Ω shunt resistor.

TABLE I. Properties of the used substrates, transducer film materials, and air at 25 °C.

	Density ρ [kg/m^3]	Specific heat capacity c_p [J/kg·K]	Heat conductivity λ [W/K·m]
		Substrate	
Quartz glass (Herasil 2)	2210	954	1.38
Polycarbonate (Makrolon)	1200	1170	0.21
		Transducer film material	
Titanium	4500	523	22
ITO	7120	233	86
		Fluid	
Air	1.204	1005	0.0262

By using sinusoidal excitation without offset, and if the excitation voltage $U(t)$ and current $I(t)$ are in phase, the effective value of the converted electrical power $P_{el\,eff}$ correspond to $U \times I$ /2.

Two narrow strips of conductive silver paint on two rims of the conductive film ensured a uniform electric contact and thus a uniform current density in the conductive film. Transducers were placed into a transducer holder and contacted with small spring contacts. Figure 4(b) shows one of the tested transducer samples mounted in the transducer holder.

Precise characterization of the acoustic properties of the thermo-acoustic transducers was achieved over a wide frequency range using a laser vibrometer as microphone (see Fig. 5). The application of a laser vibrometer for the determination of sound particle velocity amplitude using an ultralight membrane was described and tested for audible frequencies by Leclère and Laulagnet,[20] who stated that the relationship between the measured velocity amplitude v_m of the polymer membrane inserted into the sound field and the real sound particle velocity amplitude v_{ac} of the incident sound wave of frequency f can be calculated as follows:

$$v_{\text{ac}} = v_m \times \sqrt{1 + \frac{(2 \times \pi \times f \times m_m)^2}{(2 \times \rho \times c)^2}}, \quad (46)$$

where c is the sound velocity, ρ the density of the fluid, and m_m the membrane mass per unit area.

Our earlier work[21,22] showed that a laser vibrometer is well suited for the precise determination of sound particle velocity for frequencies up to 350 kHz. In this work, we expanded this method up to 1 MHz.

By applying the standard setup of Leclère and Laulagnet,[20] we observed standing waves between transducer and membrane, and the interferences that occur when the incident angle α (see Fig. 5) is equal to zero. To avoid these interferences, the transducer should be placed such that standing waves will not arise between it and the membrane. We therefore had to address different incident angles, and thus modified the formula of Leclère and Laulagnet for the determination of sound particle velocity for oblique incident waves, as follows:

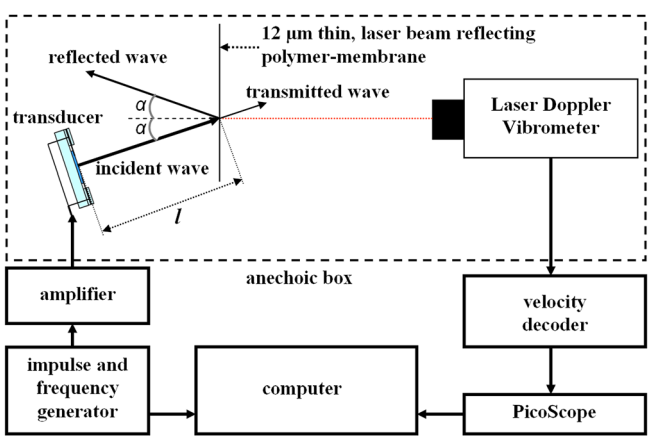

FIG. 5. Experimental setup for measuring the sound particle velocity using a Laser Doppler Vibrometer.

TABLE II. Sample properties, and excitation and measurement parameters.

Sample	a	b	c	d
Size [mm]	4.5×5	9×14	22×24	15×20
Substrate material	Quartz glass	Quartz glass	Quartz glass	PC
Film material	Ti	ITO	Ti	ITO
d_{film} [nm]	30 ± 1	300 ± 10	20 ± 1	30 ± 3
$P_{el\ eff}$ [W]	2.32 ± 0.05	1.04 ± 0.05	4.5 ± 0.05	1 ± 0.05
U [V]	25 ± 0.1	13.5 ± 0.1	27 ± 0.1	14.8 ± 0.1
I [mA]	185 ± 5	155 ± 5	335 ± 5	135 ± 5
l [mm]	20 ± 1	30 ± 1	45 ± 2	45 ± 2
α [°]	0	0	32 ± 2	25 ± 2

$$v_{ac} = v_m \times \sqrt{\frac{1}{\cos^2\alpha} + \frac{(2 \times \pi \times f \times m_m)^2}{(2 \times \rho \times c)^2}}, \qquad (47)$$

where α describes the incident angle of the sound wave to the normal of the membrane (see Fig. 5).

To minimize the influence of external sound sources, all measurements of generated sound pressures were performed in a closed anechoic box.

Figure 5 schematically shows the experimental setup and explains the measurement principle of using a single-point laser vibrometer.

From the point view of laser beams focused on the membrane (focus spot of the used vibrometer $\approx 25\ \mu$m), the incident sound waves can be regarded as quasi-plane waves. Hence, multiplying the amplitude of the sound particle velocity v_{ac} by the acoustic impedance of the fluid yields the sound pressure amplitude at the measurement point,

$$\Delta p = \Delta v_{ac} \times Z_{fluid} = \Delta v_{ac} \times \rho_{fluid} \times c_{fluid}. \qquad (48)$$

The sound pressure level L in air is defined as

$$L_A[\mathrm{dB}] = 20 \times \log(\Delta p / p_0) \text{ with } p_0 = 20 \times 10^{-6}\ \mathrm{Pa}. \qquad (49)$$

IV. RESULTS

A. Excitation with continuous sinusoidal power

All samples were excited using a continuous sinusoidal voltage without offset and with constant amplitude in a frequency range up to 1 MHz.

Figure 6 compares the analytically predicted and the measured sound pressure levels with respect to the thermal excitation frequency f_{th} for four different transducer samples.

Excellent agreement is shown between the analytical and the experimental curves. The slight oscillations with a maximum amplitude of about 3 dB can be assigned to standing waves due to the perpendicular alignment of the transducer direction and the sensing polymer membrane (incident angle $\alpha = 0$). This effect was diminished by increasing α, as can be observed in Figures 6(c) and 6(d). The investigated frequency range is limited at high frequencies due to the noise of the measurement system. The frequency-dependent noise level is additionally plotted in the diagrams. For high-frequency applications, the effect of sound attenuation as given in Eq. (30) cannot be neglected. At distances of about

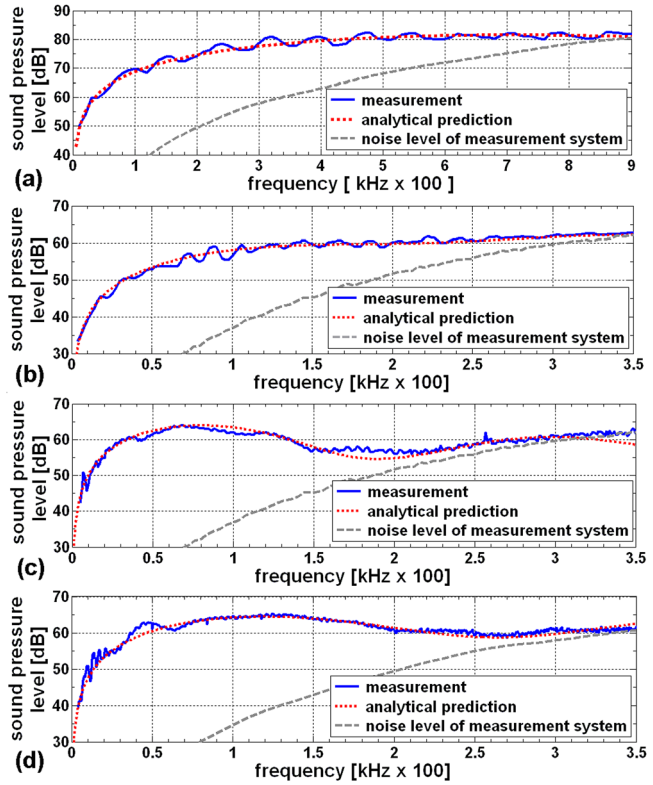

FIG. 6. Comparison of measured (solid line) and calculated (dotted line) sound pressure levels with respect to operating frequency for samples (a)–(d) (sample properties, excitation, and measurement parameters are listed in Table II). Dashed line represents the noise level of the measurement system.

6 cm, the sound pressure was already found to be attenuated by a factor of almost 10 dB at 1 MHz. Therefore, we reduced the transducer–membrane distance l for the smallest transducer sample (a) to about 20 mm.

Figure 6 shows also that the thermo-acoustic transducer on the polycarbonate substrate (sample d) generated comparable sound pressure levels to the transducer on quartz glass (sample c), but consumed only a quarter of the electric power due to the smaller thermal effusivity of the substrate.

The slight deviations from the calculated sound pressure levels for the 22×24 mm transducer sample c resulted from the inexact positioning of the transducer relative to the measurement point. As Figure 7 shows, the sound fields generated by the transducers are very complex. Small variations in the positioning of the transducer (± 1 mm), especially during measurements in the near field (see Figure 7(b)), can lead to significant deviations from the expected sound pressures.

The near-field effect can be observed in Figures 6(c) (at 200 kHz) and 6(d) (at 260 kHz). The deviations of the linear frequency characteristics occur due to the changes of wavelength in conjunction with the corresponding spatial shift of destructive and constructive interferences of the generated waves. These also can be seen in Figure 7, which shows the sound pressure distribution including the near field in air calculated using Eq. (34) for the smallest (sample a) and for the largest (sample c) thermo-acoustic transducer samples on quartz glass substrates under continuous sinusoidal excitation without offset at constant frequency and input power. Here, we represent the generated sound fields.

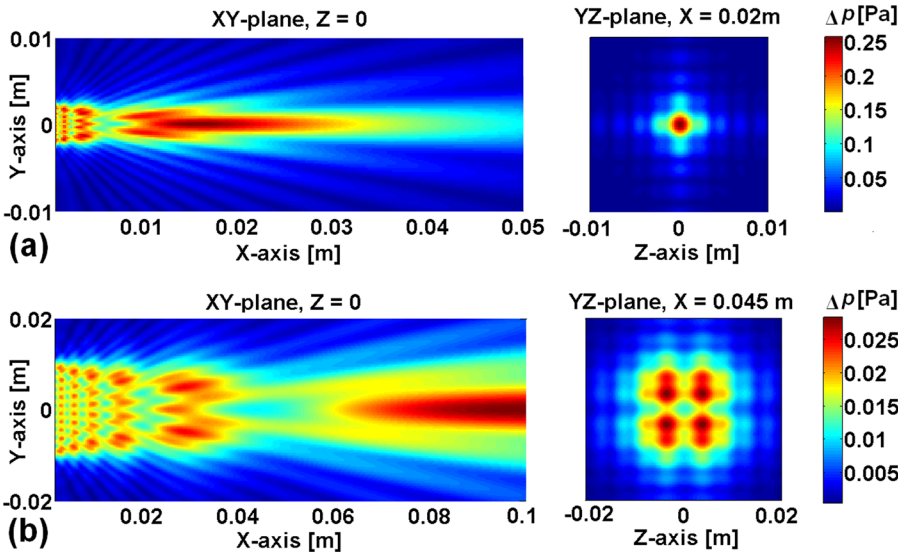

FIG. 7. Sound pressure distributions in the XY- and YZ-planes calculated using Eq. (34) for transducers placed at zero in the YZ-plane: (a) a 4.5×5 mm transducer (sample a) at 750 kHz 2.32 ± 0.02 W_{eff} sinusoidal excitation without offset; and (b) a 22×24 mm transducer (sample c) on a quartz glass substrate at 200 kHz 4.5 ± 0.02 W_{eff} sinusoidal excitation without offset.

B. Single-impulse excitation

Figure 8 compares the measured velocity $v_m(t)$ of a sensing polymer membrane after a single 500 ns impulse excitation of $U_{el} = 1.5$ kV and $I_{el} = 5$ A from two conventional piezoelectric airborne transducers and a 1×1 cm thermo-acoustic transducer of 30 nm-thin titanium film on a quartz glass substrate. The non-focusing AirTech 200 conventional transducer had an active area of about 1.1 cm^2; that of the focusing Ultran GN-55 conventional transducer was about 4 cm^2. Each transducer was tested at a distance of 60 ± 3 mm from the sensing polymer membrane.

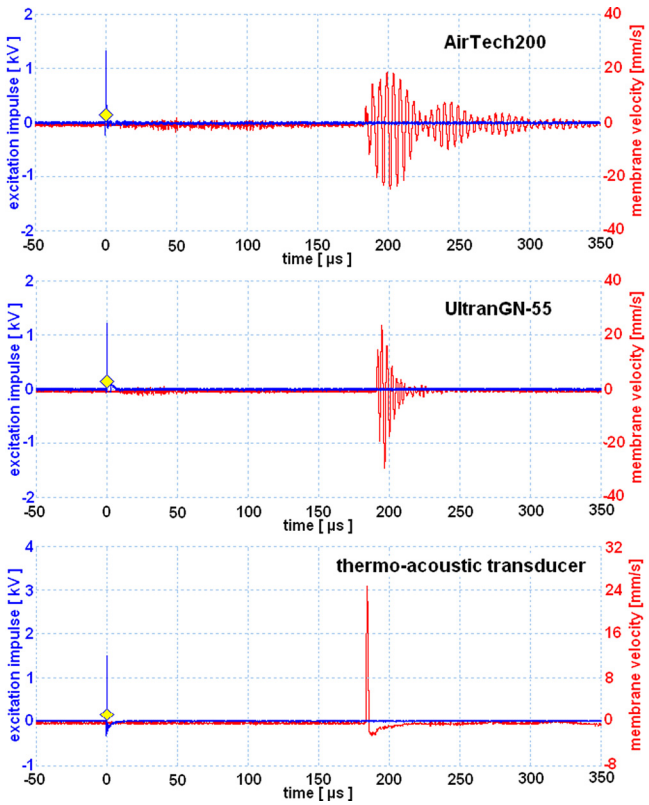

FIG. 8. Comparison of measured membrane velocity after excitation with (from top to bottom) AirTech 200, Ultran GN-55, and thermo-acoustic airborne ultrasound transducers placed 60 ± 3 mm from the membrane. Transducers were excited with 1.5 kV 500 ns impulses. The mass of polymer membrane was 12,641 g/m^2.

As expected, the conventional piezo-electric transducers showed typical resonant behavior with long post-oscillations after the short impulse excitation (Figure 8), but the thermo-acoustic transducer generated a single sound impulse free from any post-oscillations.

Figure 9 compares the acoustic spectra and effective sound pressure levels at frequencies up to 1 MHz for the same three transducers. The conventional transducers showed maximum sound pressures of about 140 dB at their center frequency. Their spectra are relatively narrow banded. The thermo-acoustic transducer achieved a sound pressure of 140 dB for frequencies above 0.5 MHz; it had a sound pressure of 135 dB at 300 kHz. The results clearly demonstrate that thermo-acoustic transducers can show acoustical efficiencies comparable to those of conventional piezoelectric transducers and that they could be used, unlike conventional transducers, as broadband, non-resonant ultrasound sources.

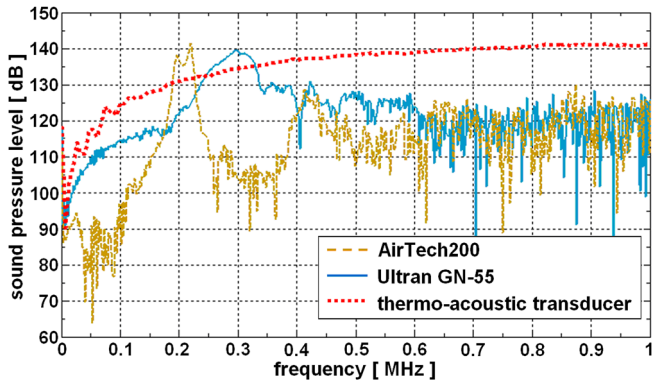

FIG. 9. Comparison of the generated sound pressure levels (effective values) at 60 mm distance from the transducers after a single 1.5 kV excitation of 500 ns duration.

V. CONCLUDING REMARKS

We propose a new model of thermo-acoustic sound generation based only on energy consideration; it combines the thermal and acoustical properties of sound waves.

The motivation for this energy-based method is that the thermo-acoustic effect, in fluids as well as in solids, cannot be handled either purely thermally or purely acoustically. The transition of thermal energy into directed kinetic energy of particle ensembles is a statistical phenomenon. This can be described by Bose-Einstein statistics and is—even as a non-trivial approach—a commonly used tool of condensed matter physics. Hence, the thermo-acoustic effect joins the group of coupled acoustical phenomena such as the electromagnetic and the laser induced sound generation. All these methods have in common, that the local change of electromagnetic or thermal energy at the μs- and ns-timescale, leads to the local energy density fluctuation, generating quasi-particles like phonons. However, the description of a single phonon and its behavior at the ps- and fs-timescale is clearly beyond of the scope of this work.

This work shows, both analytically and experimentally, that thermo-acoustic transducers are suited to broadband ultrasound generation; have an acoustical efficiency comparable to that of their conventional counterparts; and that optimized thermo-acoustic transducers could be developed to be better than conventional ultrasound transducers.

Possible optimizations include focusing designs, optimizing the transducer film materials (CNTs, graphene), and using substrates with lower thermal effusivities. Such substrates could be porous, such as the porous silicon substrates already proposed by Shinoda *et al.*[5] or aerogels and xerogels.

Our earlier works[21,22] have examined the properties of thermo-acoustic transducers consisting of free-hanging carbon nano-fibers and carbon nano-fibers on ceramics with small effusivity. These materials were shown to be suitable for efficient ultrasound generation, but they showed some practical disadvantages, such as chemical, thermal, and mechanical instability. Therefore, thermo-acoustic transducers based on graphite are, to the best of our knowledge, unsuitable for high-performance ultrasound applications.

With respect to the theoretical basis, our model shows a linear dependence on f_{th} for the generated sound pressure, unlike the works of Arnold and Crandall[2] and Xiao.[7,8] However, we note that Arnold and Crandall developed their model for low frequencies up to a few kHz.

The works of Vesterinen *et al.*,[14] Shinoda *et al.*,[5] and Boullosa and Santillan[6] also show that the linear approach seems to be correct.

Being more precise, our findings show that for large C_{film} the square root term of f_{th} in the energy distribution coefficients E (Eqs. (19) and (20)) cannot be neglected, which leads to a significant deviation from linearity towards the square root dependence predicted by Arnold and Crandall.

We also compared the predictions of our analytical model with experimentally detected sound pressures from the thermo-acoustic transducers of Shinoda *et al.*,[5] Boullosa and Santillan,[6] Xiao *et al.*,[7,8] Niskanen *et al.*,[9] Aliev *et al.*,[10] Tian *et al.*,[11,12] Vesterinen,[14] Asamura *et al.*,[23] Kontomichos *et al.*,[24] Suzuki *et al.*,[25] and Suk *et al.*,[26] and found a good agreement with their experimental results.

The main parameters affecting the efficiency of thermo-acoustic transducers on substrates are the ratio of the thermal effusivities of the substrate and the surrounding fluid, the input power, the thermal excitation frequency, the sound velocity, and the heat capacity of the transducer film.

Many applications, such as medical surveys, non-destructive testing, and flow velocity determination, would also require broadband sensing.

Thermo-acoustic transducers can also be used as sensing devices such as temperature sensors, pressure sensors, sound particle velocity, and flow sensors (hot-wire and hot-film anemometry). Hot-wire-based sound particle velocity sensors, which can be used as microphones, cover a frequency range up to few kHz.[27] However, they have some practical disadvantages such as fragility, low sensitivity, and high noise at the higher frequencies. Consequently, the broadband detection of sound pressures is presently much more challenging than broadband emission.

Even if the sensing part of broadband ultrasonic detection is not yet completely solved, this work shows at least the feasibility of broadband ultrasonic sound field generation in the sub-MHz range and above. This suggests the possibility of non-destructive testing applications, where a short impulse length is key for reliable defect detection.

ACKNOWLEDGMENTS

We thank our colleagues Uwe Beck, Thorid Lange, and Matthias Weise from the BAM, Department for Surface Technology for manufacturing the transducer samples and for many fruitful discussions.

APPENDIX A: GENESIS OF A SOUND WAVE USING AN ELECTRICALLY CONDUCTIVE FILM AS A THERMAL POWER SOURCE

Electro-thermo-acoustic transducers work without any macroscopic moving parts. They generate "Joule heating" ΔQ that is equal to internal energy $\Delta \check{U}$. Due to their ohmic resistance, they transform electric energy, which is equal to the kinetic energy of the electrons, into an increase of the kinetic energy of the atoms in the transducer film. Adjacent particles (molecules or atoms) colliding with the "warm" film atoms gain some of their kinetic energy, and so cool the film. The increase of kinetic energy of the adjacent particles is the directed sound particle velocity that will be transmitted to the next particles and travel away from the heat source. All the particles, which simultaneously carry an extra kinetic impulse away from the heat source, build the sound wave.

APPENDIX B: DETERMINATION OF THERMODYNAMIC EQUILIBRIUM TEMPERATURE T_{eq}

The part of the thermal energy flowing into the solid substrate Q_{sub} generates sound waves. However, given the high reflection coefficient for an acoustic wave at a solid–fluid transition (e.g., for glass-to-air the reflection coefficient ≈ 1), these waves propagate back and forth inside the substrate and slowly dissipate. Their thermal energy Q_{sub}, in

addition to the energy Q_{film} remaining in the film itself, quasi-constantly heat the substrate and its immediate surroundings. This "dc" heat will be removed in air by photonic radiation and convection (the heat conductivity of air $\lambda_{air} = 0.024$ can be neglected).

Therefore, to determine the equilibrium temperature of the transducer, we use the effective value of the thermal power that flows into the substrate and the thermal power remaining in the film,

$$P_{sub} + P_{film} = P_{out} = P_{convection} + P_{photons}, \quad \text{(B1)}$$

$$P_{fliud} = P_{el\,eff} \times E_{fluid}, \quad \text{(B2)}$$

$$P_{sub} + P_{film} = P_{el\,eff} \times (1 - E_{fluid}), \quad \text{(B3)}$$

$$P_{convection} = h_{c\,air} \times (T_{sub+film} - T_{0\,air}), \quad \text{(B4)}$$

where $h_{c\ air}$ is the convection constant.

$$P_{photons} = \varepsilon_{sub+film} \times \sigma \times S_{sub+film} \times (T^4_{sub+film} - T^4_{0\,\mathrm{air}}) \quad \text{(B5)}$$

(ε is the emissivity of the material and $\sigma = 5.670373(21) \times 10^{-8}$ W·m^{-2}·K^{-4} is the Stefan–Boltzmann constant),

$$P_{sub} + P_{film} = \varepsilon_{sub+film} \times \sigma \times S_{sub+film} \times (T^4_{sub+film} - T^4_{0\,air}) + h_{\mathrm{c\ air}} \times S_{sub+film} \times (T_{sub+film} - T_{0\,air}). \quad \text{(B6)}$$

Solving Eq. (B6) for $T_{sub+film}$ yields the equilibrium temperature of the substrate, the transducer film, and also the surrounding air layer close to the transducer. For example, consider a flat glass substrate body with a total area of 2 cm^2 and emissivity $\varepsilon = 0.95$ in static air at room temperature (293.15 K, 20 °C) being heated constantly with 1 W effective power. Assuming the convection constant of static air $h_{c\ air} = 20$ (EN ISO 6946 norm), in a few minutes the transducer will reach its equilibrium temperature T_{eq} of about 452.19 K (179.4 °C).

APPENDIX C: DETERMINATION OF THE ENERGY $Q_{photons\,th}$ TRANSPORTED BY PHOTONS

Consider, for example, a 30 nm-thin titanium film covering 1 cm^2 on a quartz glass being excited for $t_{th} = 100\ \mu$s (10 kHz) with 10 W effective power, $Q_{th} = 1 \times 10^{-3}$ J. Using thermal diffusion $a = \lambda/(\rho \times c_p)$, the heat penetration depth $d_{th} = (a \times t_{th}/2 \times \pi)^{1/2}$, and the density ρ we can determine the mass of the heated fluid and the substrate layers during one heating period t_{th}:

$$M_{sub} = d_{th\,sub} \times \rho_{sub} \times S_{film},\ M_{fluid} = d_{th\,fluid} \times \rho_{fluid} \times S_{film}.$$

The maximum temperature rise of the film above the initial room temperature ($T_0 = 293.15$ K) will be $\Delta T_{film} = Q_{th}/(c_{p\ film} \times M_{film} + c_{p\ \ sub} \times M_{sub} + c_{p\ \ fluid} \times M_{fluid}) = 1.4$ K. The maximum of both sides, from the transducer film, transported energy by photons during 100 μs, will be $Q_{photons\,th} = \varepsilon \times \sigma \times S_{film} \times ((\Delta T + T_0)^4 - T_0^4) \times t_{th} = 1.4 \times 10^{-7}$ J (ε is the emissivity of the transducer material, $\sigma = 5.670373(21) \times 10^{-8}$ W × m^{-2} × K^{-4} is the Stefan–Boltzmann constant, and $S_{film} = 2 \times 1$ cm^2 is the total transducer film surface). This represents 0.014% of the total input energy Q_{th}. For 10 μs continuous excitation (100 kHz) with 10 W effective power, the maximum energy transported by photons $Q_{photons\,th}$ is only 0.004%, and for 1 μs (1 MHz) continuous excitation $Q_{photons\,th}$ is only 0.001% of the input energy $Q_{th\,in}$. Therefore, the photonic part $Q_{photons\,th}$ can be neglected.

[1] P. de Lange, "On thermophones," Proc. R. Soc. London **91**(628), 239–241 (1915).
[2] H. D. Arnold and I. B. Crandall, "The thermophone as a precision source of sound," Phys. Rev. **10**(1), 22–38 (1917).
[3] E. C. Wente, "The thermophone," Phys. Rev. **19**(4), 333–345 (1922).
[4] W. Geffcken and L. Keibs, "Untersuchungen über akustische Schwellenwerte. II. Das Thermophon und seine Verwendung als akustisches meßinstrument," Ann. Phys. **408**, 404–430 (1933).
[5] H. Shinoda, T. Nakajima, K. Ueno, and N. Koshida, "Thermally induced ultrasonic emission from porous silicon," Nature **400**, 853–855 (1999).
[6] R. R. Boullosa and A. O. Santillan, "Ultrasound radiation from simple thermoacoustic transducer," Acta Acustica united with Acustica **90**, 277–284 (2004).
[7] L. Xiao *et al.*, "Flexible, stretchable, transparent carbon nanotube thin film loudspeakers," Nano Lett. **8**(12), 4539–4545 (2008).
[8] L. Xiao *et al.*, "High frequency response of carbon nanotube thin film speaker in gases," J. Appl. Phys. **110**, 084311 (2011).
[9] A. O. Niskanen *et al.*, "Suspended metal wire array as a thermoacoustic sound source," Appl. Phys. Lett. **95**, 163102 (2009).
[10] A. E. Aliev, M. D. Lima, S. Fang, and R. H. Baughman, "Underwater sound generation using carbon nanotube projectors," Nano Lett. **10**, 2374–2380 (2010).
[11] H. Tian *et al.*, "Graphene-on-paper sound source devices," ACS Nano **5**(6), 4878–4885 (2011).
[12] He Tian *et al.*, "Transparent, flexible, ultrathin sound source devices using indium tin oxide films," Appl. Phys. Lett. **99**, 043503 (2011).
[13] F. A. McDonald and G. C. Wetsel, "Generalized theory of the photoacoustic effect," J. Appl. Phys. **49**(4), 2313–2322 (1978).
[14] V. Vesterinen, A. O. Niskanen, J. Hassel, and P. Helistö, "Fundamental efficiency of nanothermophones: Modeling and experiments," Nano Lett. **10**, 5020–5024 (2010).
[15] H. Hu and Y. Wang, "Analysis of thermal-mechanical coupling and thermal wave penetration depth for thermo-acoustic emission," in *ASME Conference Proceedings, IMECE 2011* (2011), Vol. 8, pp. 647–656.
[16] H. Hu, Y. Wang, and Z. Wang, "Wideband flat frequency response of thermo-acoustic emission," J. Phys. D: Appl. Phys. **45**, 345401 (2012).
[17] R. R. Boullosa and A. O. Santillan, "A note on the use of novel thermoacoustic radiators for ultrasonic experiments: The importance of phase in a focused field," Eur. J. Phys. **27**, 95–102 (2006).
[18] L. van der Tempel, G. P. Melis, and T. C. Brandsma, "Thermal conductivity of a Glass: I. Measurement by the glass–metal contact," Glass Phys. Chem. **26**(6), 606–611 (2000).
[19] *VDI-Wärmeatlas: Berechnungsblätter für den Wärmeübergang, 9 Auflage* (VDI-Verlag, Düsseldorf, 2002).
[20] Q. Leclère and B. Laulagnet, "Particle velocity field measurement using an ultra-light Membrane," Appl. Acoust. **69**, 302–310 (2008).
[21] A. Harrer, M. Daschewski, J. Prager, M. Kreutzbruck, M. Guderian, and A. Meyer-Plath, "Thermoacoustic generation of airborne ultrasound using carbon materials at the micro- and nanoscale," Int. J. Appl. Electromagn. Mech. **39**(1–4), 35–41 (2012).
[22] M. Daschewski, A. Harrer, J. Prager, M. Kreutzbruck, A. Meyer-Plath, and M. Guderian, "Carbon nanomaterials as broadband airborne ultrasound transducer," AIP Conf. Proc. **1433**, 624–627 (2011).
[23] N. Asamura *et al.*, "Intensifying thermally induced ultrasound emission," in *Proceeding of Technical Digest Sensors Symposium* (2002), Vol. 19, pp. 477–482.
[24] F. Kontomichos, A. Koutsiobas, J. Mourjopoulos, N. Spiliopoulos, and A. Vradis, "A thermoacoustic device for sound reproduction," J. Acoust. Soc. Am. **123**(5), 3707 (2008).
[25] K. Suzuki *et al.*, "Study of carbon-nanotube web thermoacoustic loud speakers," Jpn. J. Appl. Phys. Part 1 **50**, 01BJ10 (2011).
[26] J. W. Suk *et al.*, "Thermoacoustic sound generation from monolayer graphene for transparent and flexible sound sources," Adv. Mater. **24**, 6342–6347 (2012).
[27] C. G. Lomass, *Fundamentals of Hot-Wire Anemometry* (Cambridge University Press, 1986).